Applied Catalysis B: Environmental 324 (2023) 122264

Contents lists available at ScienceDirect

Applied Catalysis B: Environmental

journal homepage: www.elsevier.com/locate/apcatb

Engineering palladium nanocrystals boosting C−C coupling by photocatalysis

Yuqing Ren, Yao Chen, Qingfei Zhao, Zhenmin Xu, Meijun Wu, Zhenfeng Bian *

MOE Key Laboratory of Resource Chemistry and Shanghai Key Laboratory of Rare Earth Functional Materials, Shanghai Normal University, Shanghai 200234, China

ARTICLE INFO

Keywords:
Photocatalysis
Palladium nanoparticles
C−C coupling
Crystalline facts control

ABSTRACT

As a typical C-C coupling catalyst, the exposed crystalline facets of palladium nanoparticles (Pd NPs) greatly affect the selectivity and activity of the reaction. Here, we utilize a pioneering photocatalytic dissolution technique to controllably expose specific crystalline facets on Pd NPs. This top-down etching scheme selectively passivates the edges of single-crystal Pd nanocubes and exposes the {111} facets, which results in an 84% increase in photocatalytic Suzuki coupling reaction yields. Moreover, this approach is also applicable to improve the activity of commercial Pd/C, and Pd/Al_2O_3 catalysts. This technique is expected to open a new path in the field of nanoparticle crystallographic conversion.

1. Introduction

Due to the advantages of small size and large surface area, precious metal nanoparticles (NPs) have attracted extensive attention for their excellent catalytic properties [1–3]. When catalytic reactions are being conducted, the reaction energies and rates of precious metal NPs are significantly associated with their exposed crystalline surfaces. [4–6]. Therefore, it is a key strategy of scientific research to further improve the catalytic performance by regulating the nanocrystal crystallographic surface [7,8]. Palladium (Pd) catalysts, which are commonly used in organic coupling reactions, are used as an example [9–16]. By using the seed-mediated method, *Jin* et al. were able to obtain Pd polyhedrons with precisely controlled sizes, shapes, and varied proportions of {100} to {111} facets on the facets. The Pd nanocubes (NCs) of slight truncation at the corners with the mixture of {100} and {111} facets, which demonstrated the optimal catalytic activity for formic acid oxidation catalysis with a balance of current density and operating potential [17]. Xie et al. synthesized sunk Pd NCs with {730} high-index facets by the method of reduction kinetic synthesis. Compared with Pd NCs enclosed by {100} facets and commercial Pd/C, their electrocatalytic activity and methanol oxidation stability are much higher [18]. Most commonly, bottom-up methods such as seed-mediated methods are used to construct precious metal nano-catalysts with specific crystalline surface exposure [19]. However, these methods require more intricate preparation steps and higher precision equipment [20,21]. Therefore, the effective construction of the desired crystalline surfaces of precious metal nanocrystals in a simple and controllable manner is crucial to regulate their catalytic properties.

In contrast to the above process is the top-down etching technique, which is also a method that enables the creation of unique crystalline NPs [22,23]. Crystalline surface modulation of precious metal NPs involves thermodynamic, kinetic, and oxidative etching mechanisms. Through literature investigation, the existing etching techniques include the thermochemistry method [24], the acid etching method [25], the self-sacrificial template method [26,27], etc. However, the thermochemistry method has high requirements for equipment, and the reaction is not easy to control. The acid etching method reacts violently, the operation is dangerous, and pollutes the environment. While the cost of the self-sacrificial template method is high. Ma et al. used deionized water, sodium chloride solution, and ferric chloride ($FeCl_3$) solution with an electron beam to investigate the oxidative etching of Pd nanorods, respectively. The synergistic effects of structural properties and solution chemistry in the etching of multi-twinned nanoparticles (MTPs) were revealed [28]. Zhang et al. controlled the shape evolution of the Pd NPs by adjusting the concentration of added hydrochloric acid. The catalytic activity of the Pd NPs was also demonstrated to be strongly dependent on the exposed facets of the surface by formic acid oxidation experiments [29]. Given the chemical inertness of precious metals, the etching process often requires oxidation with high-risk reagents or disproportionation with expensive homologous ions to obtain morphology-changing NPs. Recently, our group has proposed photocatalytic dissolution technology for precious metals, which is combined

* Corresponding author.
E-mail address: bianzhenfeng@shnu.edu.cn (Z. Bian).

https://doi.org/10.1016/j.apcatb.2022.122264
Received 31 October 2022; Received in revised form 1 December 2022; Accepted 3 December 2022
Available online 6 December 2022

with green solar energy and appropriate solvents, can not only improve the species and selectivity of precious metals but is also expected to be applied to the etching of nano-precious metal materials [30–32].

In this work, Pd NCs with uniform morphology were prepared by the liquid phase reduction method. The crystal surface changes of this typical sample were studied in detail by photocatalytic dissolution technology. Depending on the arrangement of the atoms, Pd atoms with large exposed surfaces at the top corners and edges are preferentially dissolved, resulting in Pd NPs with different morphologies and crystalline surfaces at different times. Further, the catalytic activities of Pd NPs with different crystal surfaces were compared to the Suzuki reaction. It can be found that Pd NPs exposed by a certain proportion of {111} and {100} facets have a higher iodobenzene conversion. This method can also be used for the activity optimization of commercial Pd catalysts and is expected to provide new insights into the rational design of precious metal nanocatalysts.

2. Experimental

2.1. . Chemicals and materials

Polyvinylpyrrolidone [$(C_6H_9NO)n$, PVP, MW≈ 55000, AR, ≥ 99.0%, Aladdin], L-ascorbic acid ($C_6H_8O_6$, AA, AR, ≥99.0%, Aladdin), sodium tetrachloropalladate (Na_2PdCl_4, AR, ≥98.0%, Aladdin), potassium bromide (KBr, AR, ≥99.0%, Aladdin), ethanol (C_2H_5OH, AR, ≥99.7%, Adamas), titanium dioxide (TiO_2, commercial sample of Degussa P-25), iodobenzene (C_6H_5I, AR, 99%, Adamas), bromobenzene (C_6H_5Br, AR, 99%, Adamas), phenylboronic acid ($C_6H_7BO_2$, AR, ≥98%, Adamas), tetrabutylammonium bromide ($C_{16}H_{36}BrN$, AR, ≥99%, Adamas), potassium phosphate tribasic (K_3PO_4, AR, ≥99%, Adamas), mesitylene (C_9H_{12}, AR, 99%, Adamas), acetonitrile (CH_3CN, MeCN, AR, 99.9%, Adamas) and dichloromethane (CH_2Cl_2, DCM, AR, 99.5%, Adamas), 2,3-Dichloro-5,6-dicyano-1,4-benzoquinone ($C_8Cl_2N_2O_2$, DDQ, AR, ≥98%, Adamas), sodium oxalate ($Na_2C_2O_4$, AR, 98%, Adamas). All chemicals were used as received.

2.2. Synthesis of Pd nanocubes

First, PVP (105 mg), AA (60 mg), and KBr (600 mg) were weighed and the three reagents were dissolved into 8 mL of deionized (DI) water in sequence. The above reagents were mixed well by ultrasound, and then the reaction solution was stirred at 80 °C for 10 min. Next, 57 mg Na_2PdCl_4 was added into the reaction bottle and stirred at 80 °C for 3 h. Finally, the synthesized Pd NCs were washed with water 10 times to remove excess PVP and sealed in a reagent tube for preservation (shown in Fig. S1).

2.3. Photocatalytic dissolution of Pd nanocubes

2 μL of Pd NCs solution dispersed in water were sonicated and deposited on a pure carbon film (molybdenum mesh). After drying, the prepared carbon film was inserted into the transmission electron microscopy (TEM) to capture the initial state of the Pd NCs. Then, the carbon film was removed from the TEM and transferred to the small reactor. The bottom of the reactor was TiO_2 with the mixture solution of acetonitrile (MeCN) and dichloromethane (DCM) (3:1, 20 mL) as the solvent. After irradiating the sample with a 365 nm UV lamp and photocatalysis the reaction for some time, the carbon film was directly removed and dried for observation through TEM.

2.4. Preparation of UV_{Xmin}-Pd/TiO_2 catalyst

A certain amount of TiO_2 (P25) was placed in a solution of the prepared Pd NCs. After maceration for 12 h at room temperature, we used a rotary evaporator for water removal to obtain a gray-black solid powder. The resulting product was washed with water several times, centrifuged, and dried in the oven to obtain Pd/TiO_2. Then, 100 mg precursors (Pd/TiO_2) were put into a quartz bottle, and a 40 mL reaction solution (MeCN:DCM = 3:1) was added and mixed sufficiently. The reaction bottle was irradiated with a UV lamp for 20 min, 40 min, 60 min, and 80 min to obtain UV_{Xmin}-Pd/TiO_2 catalysts with different degrees of dissolution.

2.5. Preparation of UV_{Xh}-Pd/Al_2O_3 and UV_{Xmin}-Pd/C catalyst

It is similar to the preparation process of UV_{Xmin}-Pd/TiO_2, and the difference is that an amount of TiO_2 powder equal to Pd/Al_2O_3 or Pd/C was added to the reaction. After the end of the reaction, the obtained product was centrifuged, washed, dried, and named as UV_{Xh}-Pd/Al_2O_3 or UV_{Xmin}-Pd/C according to the dissolution reaction time.

2.6. Photocatalytic Suzuki reactions

Water (1.0 mL), ethanol (1.0 mL), iodinebenzene or bromobenzene (0.5 mmol), phenylboronic acid (1.2 eqiv.), tetrabutylammonium bromide (0.50 eqiv.) and potassium phosphate (3.0 eqiv.) were added in the 10 mL reaction vessel. Followed by the addition of the internal standard 1,3,5-trimethylbenzene (1.0 eqiv.), and a certain amount of the Pd catalyst (UV_{Xmin}-Pd/TiO_2, UV_{Xh}-Pd/Al_2O_3 or UV_{Xmin}-Pd/C). The mixture after ultrasonic mixing was reacted uniformly under photocatalytic conditions (LED light, λ = 365 nm, 15 mW■m^{-2}) while stirring. After the reaction, the products (biphenyl) were monitored by gas chromatography-mass spectrometry (GC-MS).

2.7. Electrochemical measurements

Photocurrent measurements were performed at room temperature using an electrochemical analyzer (CHI 660E electrochemical station) with a standard three-electrode system. Na_2SO_4 aqueous solution (0.50 M) was used as the electrolyte. The working electrode was prepared by mixing 5 mg catalyst with 20 μL polyethylene glycol solution on FTO conductive glass. A saturated calomel reference electrode (SCE) and platinum sheet (10 mm × 20 mm) were used as reference electrodes and counter electrodes respectively.

2.8. Characterization

The phase compositions of all catalysts were determined in the air by powder X-ray diffraction measurements (XRD, Rigaku D/MAX-2000). The morphologies of all composites were characterized by high-resolution transmission electron microscopy (HRTEM, JEM-2010, 200 kV) and field emission scanning electron microscopy (FESEM, JEM–ARM200F, 50 kV). The chemical properties of all samples were studied using X-ray photoelectron spectroscopy (XPS, PerkinElmer PHI 5000 C, Al Kα). The shift of the binding energy was referenced to the C 1 s level at 284.8 eV as an internal standard. UV–vis diffuse reflectance spectroscopy (DRS) was measured on a Shimadzu, UV-2600 spectroscope. Raman spectra were measured using a Dilor Labram II (250 nm laser). Raman spectrometer across the wavenumber range of 50–1000 cm^{-1}. The contents of Pd were analyzed by an inductively coupled plasma emission spectrometer (ICP). Products analysis was measured using gas chromatography-mass spectrometry (GCMS-QP2010, Shimadzu). The GC system was equipped with an SH-Rxi-5Sil-fused silica capillary column.

3. Results and discussion

3.1. Photocatalytic etching process of Pd NCs

The Pd NCs with extremely homogeneous particles were prepared by a simple chemical synthesis method, and the preparation process was shown in Fig. S1 [33]. According to the particle size statistics, the

average size of Pd NCs is about 18 nm (Fig. S2). For a more accurate observation, we designed an experimental setup and explored the changes of Pd NCs in the photocatalytic dissolution system (Fig. S3). The Pd NCs showed a complete cubic structure when the photocatalytic system was not introduced (Fig. 1**a**). With the start of the photocatalytic dissolution reaction, the originally sharp top corners on Pd NCs were blunted within 20 min (Fig. 1**b**). Further extension of the reaction time reveals that the passivated part on Pd NCs spreads to the edges of the cube (Fig. 1**c**). After 60 min of the dissolution reaction, the edges of the Pd NCs were completely etched, resulting in the formation of spherical Pd NPs (Fig. 1**d**). Continued dissolution of the Pd NPs resulted in an overall decrease in size and their shape was no longer regular (Fig. 1**e**).

Before the dissolution reaction, the Pd NCs are very regular single crystal particles and expose {100} crystal planes (Fig. 1**f**). Interestingly, the new morphology of Pd NCs fabricated by photocatalytic dissolution exposed a different crystalline surface profile (Figs. 1**g**-1**j**). We selected single Pd NCs for the calibration of the crystal facets at different dissolution times. The results showed that with dissolution, new exposed crystalline facets, {111} facets, appear on the Pd NCs. When dissolved from the top corner, the {111} facets started to appear and gradually spread to the edge position. And the originally exposed {100} facets have been kept on the Pd NCs where they are not etched. The corresponding high-resolution Fourier fast transform (FFT) maps can further verify the crystallographic transition on the Pd NCs. Typically, the samples at 40 min and 60 min of the dissolution reaction can be observed that the central part of the Pd NCs still retains a single crystal structure dominated by {100} facets, while the diffraction patterns on their corner and edge positions become different due to the appearance of {111} crystallographic facets (Fig. S4-S5). However, the slight dissolution did not affect the average particle size of Pd NCs (Fig. S6). The appearance of Pd NCs adhering to each other during dissolution is due to Oswald ripening among nanoparticles [34,35]. Therefore, we can derive the changing pattern of Pd NCs under the effect of photocatalytic dissolution (Fig. 1**k**). Firstly, the Pd atoms on the top corners of Pd NCs are preferentially dissolved (20 min); then, the dissolution occurs at the positions along the edges of Pd NCs (40 min); finally, the Pd NCs are dissolved to become smaller (60–80 min). This dissolution process coincides with the pattern of {111} crystalline surface appearance.

3.2. *Mechanism analysis of photocatalytic etching to construct Pd NCs with different crystal facets*

The reason for photocatalytic dissolution leading to {111} exposure may be related to the crystal structure of Pd NCs. The synthesized Pd NCs in this work are face-centered cubic (FCC) structures, which have different crystal orientations and planes in different directions [36]. As can be seen in Fig. 2**a**, the axis of a, b and c represent the three directions of the crystal axis along which the Pd NCs expose the crystallographic planes {100}, {010}, and {001}, respectively. In addition, the crystal facets in the summation direction of the a, b, and c axes point to {111}, which corresponds to the direction between the opposite top angles on the Pd NCs. We have specifically labeled in gold color the atoms distributed at the top corners of the Pd NCs, which are the most easily lost in photocatalytic dissolution due to the higher surface energy (Fig. 2**b**). When the reaction proceeds for 20 min, the atoms at the top corners of the Pd NCs are preferentially solvated, which in turn exposes the {111} crystal plane in this direction (Fig. 2**c**). The atoms with surface energy second to the vertex position were on the Pd NCs prongs and they were also dissolved as the reaction proceeded (Fig. 2**d**). The Pd NCs have closed equivalent {100}, {111} and {110} planes, and the plane energies of different crystal planes are arranged according to $\gamma\{110\} > \gamma\{100\} > \gamma\{111\}$ [36,37]. As a result, the surface energy of the {111}

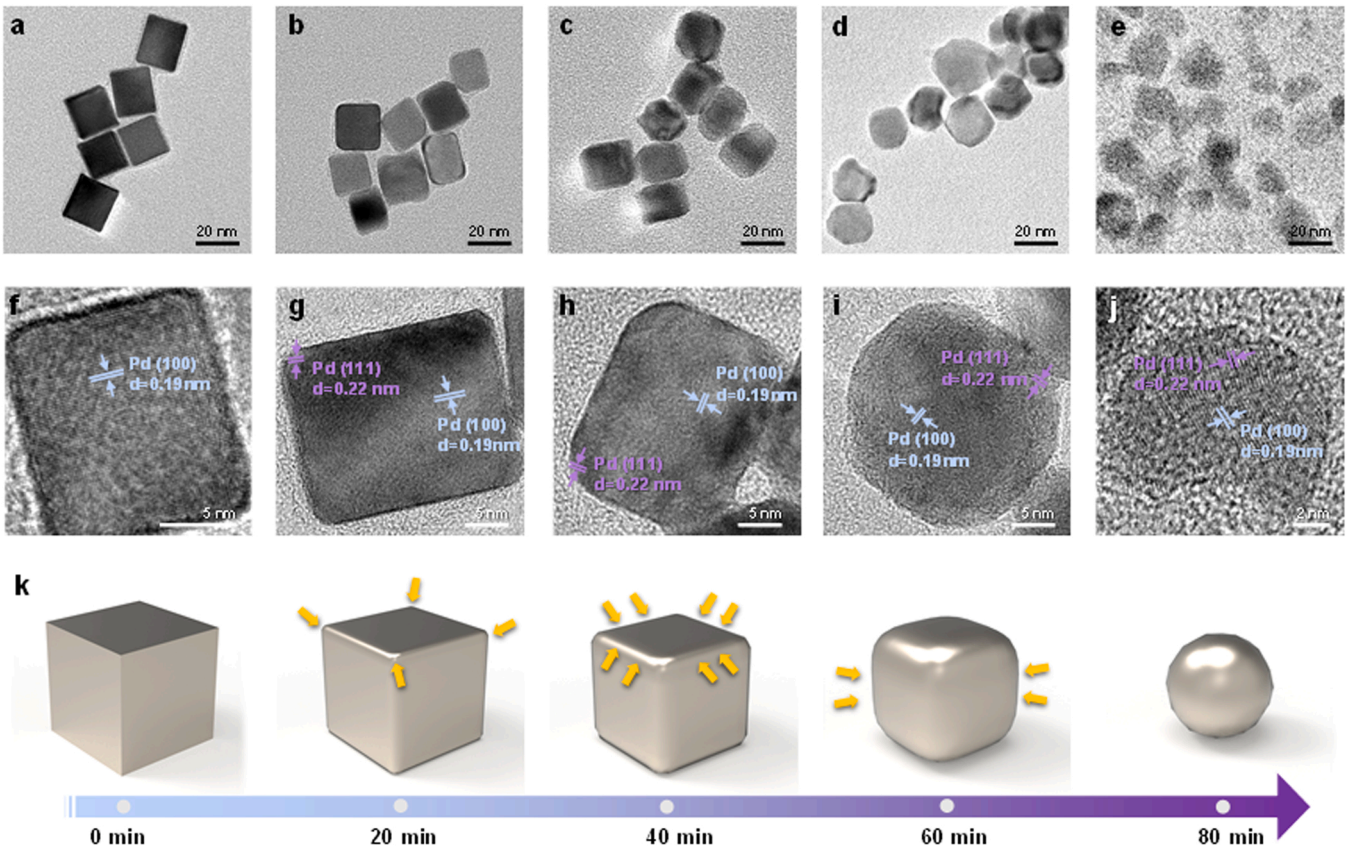

Fig. 1. Dissolution of Pd NCs at different times in the photocatalytic system. The morphological changes of Pd NCs after (a) 0 min, (b) 20 min, (c) 40 min, (d) 60 min, and (e) 80 min of the dissolution reaction. The crystal plane changes of Pd NCs correspond to different photocatalytic dissolution times at (f) 0 min, (g) 20 min, (h) 40 min, (i) 60 min, and (j) 80 min (k) Schematic diagram of Pd NCs during photocatalytic dissolution.

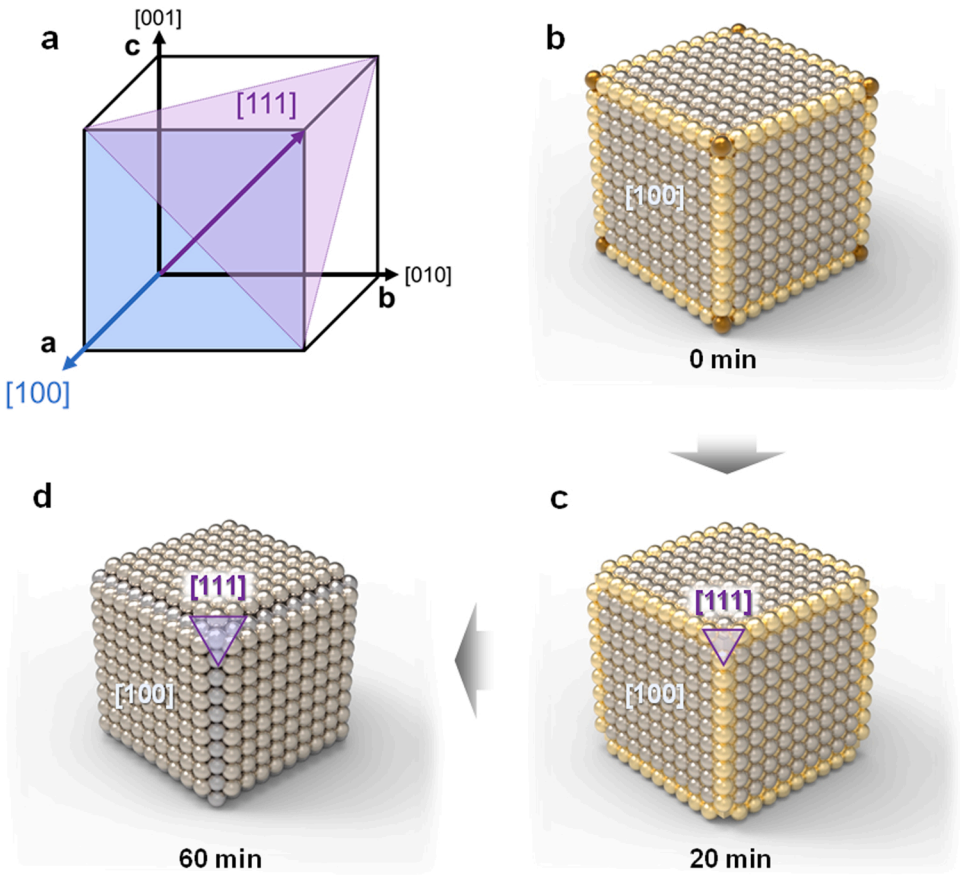

Fig. 2. Possible mechanisms for the crystal facets transformation of single-crystal Pd NCs under photocatalytic conditions. (a) The crystallographic distribution of single-crystal face-centered cubic Pd NCs. (b) Exposed crystal facets of Pd NCs before etching and the distribution of atoms with different surface energies: the golden spheres at the top corners represent the atoms with the highest surface energy on the Pd NCs, followed by yellow. (c-d) Etching of atoms on Pd NCs with the change of photocatalytic action time: the purple area is the newly exposed {111} crystal facets.

close-packed plane is lower than the {100} plane, which will gradually and partially transform the {100} plane into a more stable {111} plane [37].

3.3. Structural analysis of the UV_{Xmin}-Pd/TiO_2 catalyst

To investigate the activity of Pd NCs with different exposed crystal surfaces, we loaded Pd NCs on TiO_2 by impregnation and verified their catalytic activity by Suzuki reaction. The Pd NCs are uniformly distributed on the TiO_2 surface (Fig. 3**a**). Based on ICP measurement, the Pd content on the obtained Pd/TiO_2 varies with the dissolution time, and the dissolved content of Pd in the catalyst measured at each time point is shown in Fig. S7 and Table S1 respectively. Fig. 3**b** exhibits the XRD patterns of the Pd/TiO_2, which correspond to the anatase phase (ICSD 21–1272) and rutile phase (ICSD 21–1276) of TiO_2. And the main diffraction peaks at about 39.9°, 46.4°, and 67.8° are attributed to the Pd [37–40]. The structure of TiO_2 in the diffraction peaks of UV_{Xmin}-Pd/-TiO_2 synthesized by dissolution did not change, while the peak intensity of Pd decreased with increasing dissolution time. Similarly, the surface binding between Pd and TiO_2 resulted in a small shift in the Raman active peak of the catalyst and a significant increase in the Raman peak intensity of the catalyst before the dissolution due to the plasma response of Pd (Fig. S8). The binding between TiO_2 and Pd may change after dissolution owing to Pd is gradually oxidized from the atomic to the ionic state during the photocatalytic dissolution process. The binding energy of Pd shifts toward higher binding energy after dissolution, which indicates that Pd has bonded with TiO_2, thus favoring Pd to become an electron-rich state [41–43]. In the O 1 s spectrum of UV_{X-min}-Pd/TiO_2 (Fig. S9a), the two peaks at 530.1 and 531.6 eV in the spectrum can be attributed to the lattice oxygen and oxygen in the hydroxyl group of TiO_2, respectively. Similarly, the binding energy of O shifts to low binding energy by about 0.1–0.5 eV with the increasing photocatalytic etching time, which accounts for the formation of the Pd-O bonds [44]. The peaks of Ti are shifted about 0.3 eV toward the low binding energy, which are further evidence that Pd may have entered the lattice of TiO_2 after photocatalytic etching (Fig. S9b) [45]. In addition, Pd also enhances the light absorption of TiO_2 in the visible region, but due to the photocatalytic dissolution, the content of Pd gradually decreases and the visible light absorption gradually becomes lower (Fig. S10).

3.4. Catalytic activity of UV_{Xmin}-Pd/TiO_2

Pd catalysts have been widely demonstrated to catalyze photocatalytic Suzuki coupling reactions between phenylboronic acids and different aryl halides [19, 44–50]. TiO_2 is a typical photocatalyst that facilitates the transfer of photogenerated electrons to Pd under the action of light to promote the Suzuki reaction. Therefore, we tested the coupling reaction using UV_{Xmin}-Pd/TiO_2-catalyzed iodobenzene and phenylboronic acid under 365 nm UV light. It is noteworthy that from $UV_{0\ min}$-Pd/TiO_2 to $UV_{80\ min}$-Pd/TiO_2, the coupling reaction with different catalysts showed a trend of increasing first and then decreasing. The experimental results showed that $UV_{60\ min}$-Pd/TiO_2 had the best catalytic activity when the reaction condition was iodobenzene: phenylboronic acid = 1:1, which was about 84% higher than that of $UV_{0\ min}$-Pd/TiO_2 (Fig. 3**d**). The increase in activity was demonstrated by photoelectric testing due to the concentration of more photogenerated electrons on Pd (Fig. S11). The cycling experiments further confirmed that $UV_{60\ min}$-Pd/TiO_2 had wonderful cycling stability performance and the catalytic activity of the catalyst can still be maintained at about 96% after ten cycles (Fig. 3**e**). Furthermore, the catalyst has high generality for other halogenated benzene. The different catalytic activities of Pd NCs with various degrees of crystalline surface exposure for bromobenzene and chlorobenzene may be related to the activation ability of

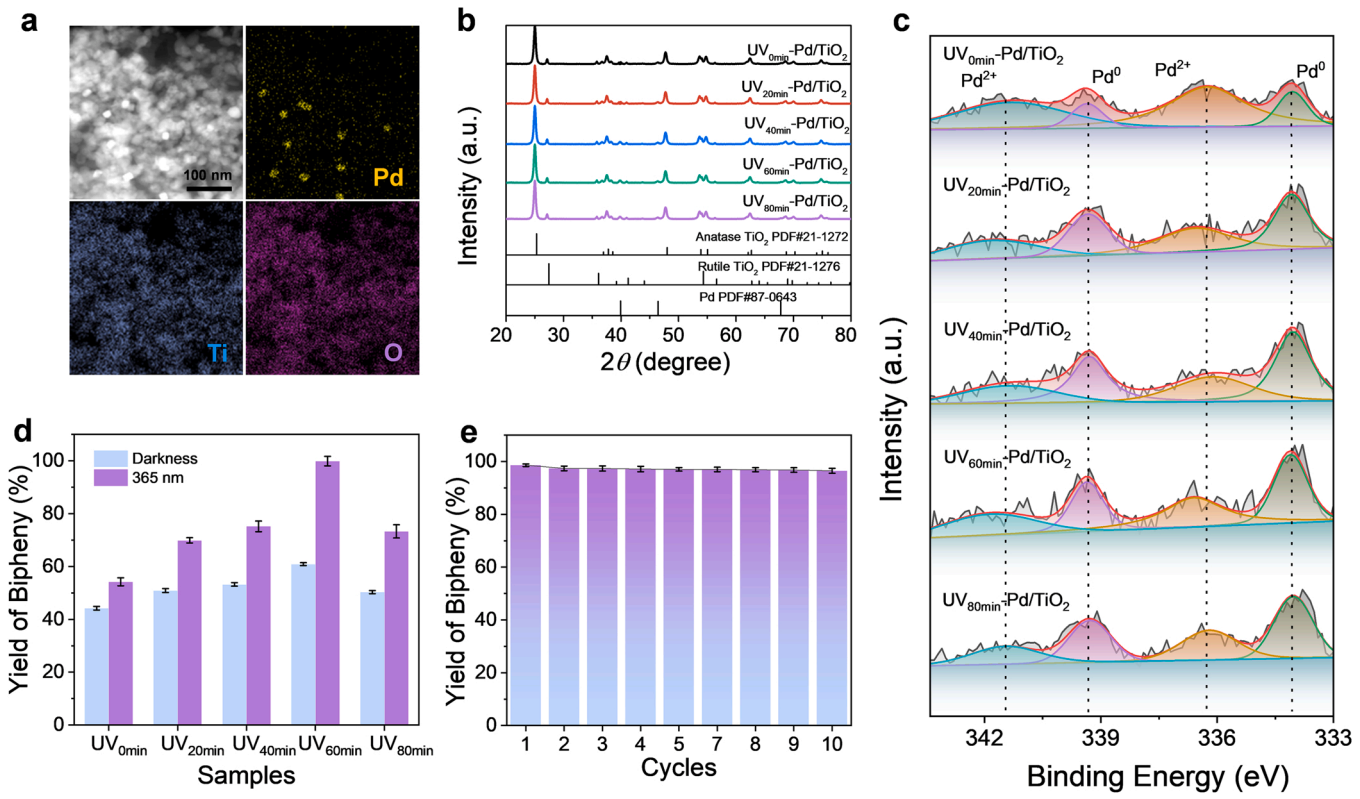

Fig. 3. (a) HADDF-EDS images of Pd/TiO_2 samples. Scale bars: 100 nm. (b) The XRD patterns of UV_{Xmin}-Pd/TiO_2 catalysts. (c) The XPS survey spectra of UV_{Xmin}-Pd/TiO_2 catalysts with Pd 3d. (d) The activity of the Suzuki reaction of iodobenzene and phenylboronic acid over UV_{Xmin}-Pd/TiO_2 catalysts with and without light illumination. (e) Recyclability of the $UV_{60\ min}$-Pd/TiO_2 catalysts as the efficient catalyst for the Suzuki coupling reaction.

the crystalline surface for the reaction substrate (Fig. S12-S13). This suitable crystalline surface exposure is facilitated by the effect of photocatalytic dissolution, and Pd will be quickly and completely etched if conventional dissolution techniques such as aqua regia or nitric acid are used instead of photocatalytic dissolution (Fig. S14). As a result, the reactivity of the Pd/TiO_2 samples treated with aqua regia or nitric acid showed a significant decrease (Fig. S15). Therefore, compared with the conventional technique, the green photocatalytic dissolution technique can be used to stably construct crystallographically controllable Pd NPs for improving the activity of organic reactions [49–52].

3.5. Mechanisms of photo-enhanced Suzuki coupling reactions

Adjusting the ratio of reaction substrates and capturing intermediate active substances, we further investigated the reason for the promotion of the coupling reaction by Pd NCs. The experimental results show that when the reactants are only iodobenzene or only phenylboronic acid, the yield of self-coupling to obtain biphenyl is almost zero and the overall trend of reactivity was volcanic curve (Fig. 4**a**). Among them, the reaction activity was better when there was more phenylboronic acid than when there was more iodobenzene, suggesting that the newly exposed {111} surface may be more favorable for the adsorption of phenylboronic acid. The benzene on biphenyl is derived from iodobenzene and phenylboronic acid, respectively, so the reaction is the most active at a substrate ratio of 1:1. Furthermore, it can be seen that when DDQ was added as the electron capture agent, the product obtained at the end of the reaction was very low, indicating that electrons play a very important role in the reaction. When sodium oxalate was added as the trapping agent of holes, the reaction activity decreased, indicating that the reaction was also inhibited to a certain extent (Fig. 4**b**). Since the work function difference between Pd and TiO_2 is 0.029 eV, which allows the electrons transfer from TiO_2 to Pd NCs. The Pd NCs become electron-rich, which would be more conducive to the oxidation of aryl halides. At the same time, when the photogenerated holes generated by TiO_2 diffused to the adsorption site, the phenylboronic acid adsorbed on the surface of TiO_2 through electrostatic adsorption was oxidized and the C-B bond was broken. Ultimately, the two benzene sources are coupled to form biphenyl through the catalysis of Pd (Fig. 4**c**) [53,54].

3.6. Etching universality of photocatalytic dissolution technology for precious metal nanoparticles

We selected commercial industrial samples to further validate the universality of the photocatalytic dissolution technique for activated catalysts (Fig. 5). The experimental results showed that UV_{Xh}-Pd/Al_2O_3 catalysts and UV_{Xmin}-Pd/C obtained at different times by photocatalytic treatment have various Suzuki reaction activity. The $UV_{60\ min}$-Pd/C catalysts can increase catalytic performance by 67%, and the activity of the $UV_{2\ h}$-Pd/Al_2O_3 catalyst can be increased by about 60%. The catalytic activities of UV_{Xh}-Pd/Al_2O_3 and UV_{Xmin}-Pd/C on the coupling reaction of iodobenzene and phenylboronic acid without illumination were shown in Fig. S16. The data show that the reaction activity is stronger than that condition without illumination. So, the photocatalytic etching method has certain universality, which can be applied in practical production and life, and has certain practical significance for industrial production.

4. Conclusion

In summary, we take advantage of photocatalysis to link precious metal etching with the Suzuki coupling reaction, which is simple, safe, and environmentally friendly. Here, we have directly observed the etching process of Pd NCs under photocatalytic conditions by electron

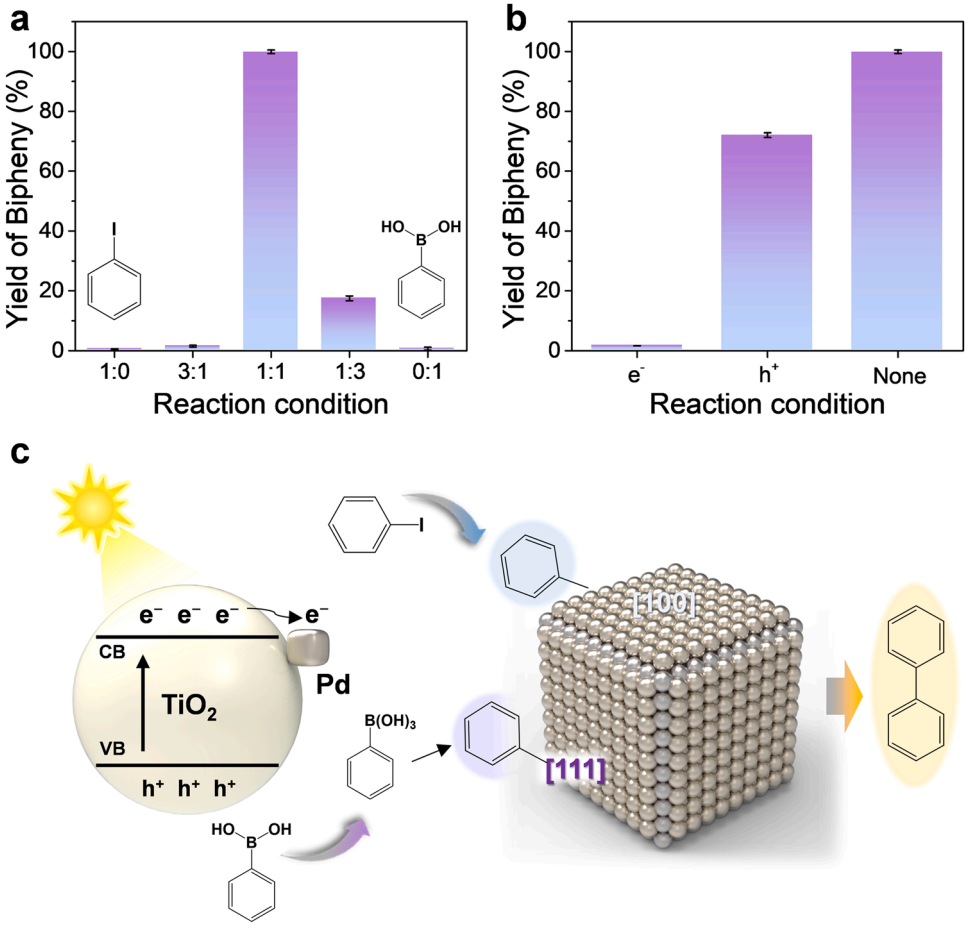

Fig. 4. (a) Photocatalytic coupling reaction activity of $UV_{60\ min}$-Pd/TiO_2 under different ratios of substrates (iodobenzene: phenylboronic acid). (b) Photocatalytic coupling reaction activity of $UV_{60\ min}$-Pd/TiO_2 in different capture experiments (electrons and holes captured by 2,3-Dichloro-5,6-dicyano-1,4-benzoquinone and sodium oxalate, respectively). (c) The mechanism of photocatalytic Suzuki reaction on the UV_{Xmin}-Pd/TiO_2 catalyst.

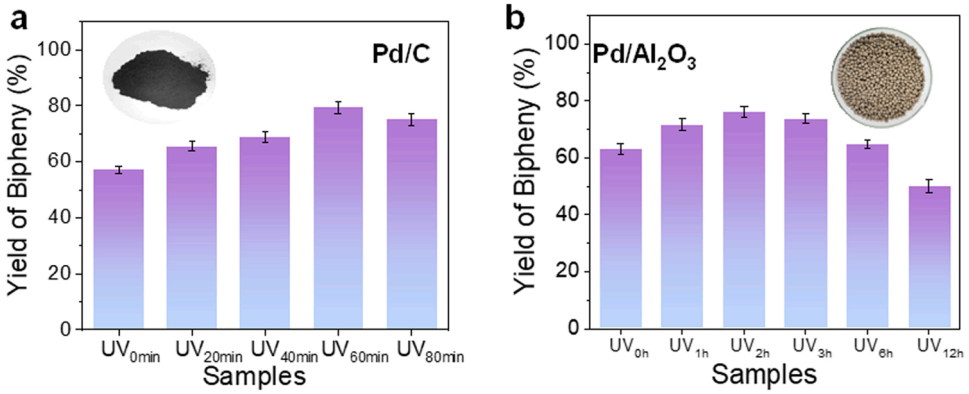

Fig. 5. Activity of commercial Pd catalysts for Suzuki coupling reactions after treatment by photocatalytic dissolution: (a) Pd/C and (b) Pd/Al_2O_3. The inserted image is the physical image of the sample before photocatalytic treatment.

microscopy. The etching process starts from the apex first, leading to the gradual exposure of new {111} crystallographic planes of Pd NCs from the cubic structure. And a series of catalysts (UV_{Xmin}-Pd/TiO_2) with different catalytic activities, were further obtained. The catalysts treated by photocatalytic technique with Suzuki reaction as the probe reaction have high selectivity. This work provides a unique perspective on the etching as well as dissolution of noble metal nanoparticles, which provides more references for future research on precious metal catalytic materials. In the follow-up optimization of the work, we will continue to explore the etching conditions and prospective applications of other precious metals.

CRediT authorship contribution statement

Yuqing Ren and Yao Chen: Conceptualization, Methodology, Software, Writing – reviewing and editing, Data curation, Writing – original draft preparation. **Qingfei Zhao, Zhenmin Xu, Meijun Wu:** Writing – reviewing and editing. **Zhenfeng Bian:** Methodology, Data

curation, Supervision, Writing – reviewing and editing,

Declaration of Competing Interest

The authors declare that they have no known competing financial interests or personal relationships that could have appeared to influence the work reported in this paper.

Data availability

No data was used for the research described in the article.

Acknowledgments

This work was supported by the National Key Research and Development Program of China (2020YFA0211004), the National Natural Science Foundation of China (22176128, 21876114), Sponsored by Program of Shanghai Academic Research Leader (21XD1422800), Shanghai Government (19DZ1205102, 19160712900), Chinese Education Ministry Key Laboratory and International Joint Laboratory on Resource Chemistry, and Shanghai Eastern Scholar Program. “111 Innovation and Talent Recruitment Base on Photochemical and Energy Materials” (No. D18020), Shanghai Engineering Research Center of Green Energy Chemical Engineering (18DZ2254200). Shanghai Frontiers Science Center of Biomimetic Catalysis.

Appendix A. Supporting information

Supplementary data associated with this article can be found in the online version at doi:10.1016/j.apcatb.2022.122264.

References

[1] J. Zhu, M. Wei, Q. Meng, Z. Chen, Y. Fan, S.W. Hasan, X. Zhang, D. Lyu, Z.Q. Tian, P.K. Shen, Ultrathin-shell IrCo hollow nanospheres as highly efficient electrocatalysts towards the oxygen evolution reaction in acidic media, Nanoscale 12 (2020) 24070–24078.
[2] T.H. Yang, J. Ahn, S. Shi, P. Wang, R. Gao, D. Qin, Noble-metal nanoframes and their catalytic applications, Chem. Rev. 121 (2021) 796–833.
[3] L. An, X. Zhao, T. Zhao, D. Wang, Atomic-level insight into reasonable design of metal-based catalysts for hydrogen oxidation in alkaline electrolytes, Energy Environ. Sci. 14 (2021) 2620–2638.
[4] J. Yun, H.S. Chung, S.G. Lee, J.S. Bae, T.E. Hong, K. Takahashi, S.M. Yu, J. Park, Q. Guo, G.H. Lee, S.Z. Han, Y. Ikoma, E.A. Choi, An unexpected surfactant role of immiscible nitrogen in the structural development of silver nanoparticles: an experimental and numerical investigation, Nanoscale 12 (2020) 1749–1758.
[5] M.E. King, M.L. Personick, Iodide-induced differential control of metal ion reduction rates: synthesis of terraced palladium–copper nanoparticles with dilute bimetallic surfaces, J. Mater. Chem. A 6 (2018) 22179–22188.
[6] Y. Shi, Z. Lyu, M. Zhao, R. Chen, Q.N. Nguyen, Y. Xia, Noble-Metal nanocrystals with controlled shapes for catalytic and electrocatalytic Applications, Chem. Rev. 121 (2021) 649–735.
[7] X.-K.G. Hengwei Wang, X. Zheng, H. Pan, J. Zhu, S. Chen, L. Cao, W.-X Li, J. Lu, Disentangling the size-dependent geometric and electronic effects of palladium nanocatalysts beyond selectivity, Sci. Adv. 5 (2019) 1–8.
[8] G. Collins, M. Schmidt, C. O'Dwyer, J.D. Holmes, G.P. McGlacken, The origin of shape sensitivity in palladium-catalyzed Suzuki-Miyaura cross coupling Reactions, Angew. Chem. Int. Ed. 53 (2014) 4142–4145.
[9] Z. Dong, A. Mukhtar, T. Ludwig, S.A. Akhade, S. Kang, B. Wood, K. Grubel, M. Engelhard, T. Autrey, H. Lin, Efficient Pd on carbon catalyst for ammonium formate dehydrogenation: Effect of surface oxygen functional groups, Appl. Catal. B Environ. 321 (2023), 122015.
[10] M. Duan, C. Hu, D. Duan, R. Chen, C. Wang, D. Wu, T. Xia, H. Liu, Y. Dai, R. Long, L. Song, Y. Xiong, Ppm-level Cu dopant on ultrathin Pd nanosheets/TiO_2 for highly enhanced photocatalytic alcoholysis of epoxides, Appl. Catal. B Environ. 307 (2022), 121211.
[11] R. Chinchilla, C. Najera, Chemicals from alkynes with palladium catalysts, Chem. Rev. 114 (2014) 1783–1826.
[12] F.S. Han, Transition-metal-catalyzed Suzuki-Miyaura cross-coupling reactions: a remarkable advance from palladium to nickel catalysts, Chem. Soc. Rev. 42 (2013) 5270–5298.
[13] I.P. Mikheenko, J.A. Bennett, J.B. Omajali, M. Walker, D.B. Johnson, B.M. Grail, D. Wong-Pascua, J.D. Moseley, L.E. Macaskie, Selective hydrogenation catalyst made via heat-processing of biogenic Pd nanoparticles and novel ‘green’ catalyst for Heck coupling using waste sulfidogenic bacteria, Appl. Catal. B Environ. 306 (2022), 121059.
[14] K. Mori, H. Hata, H. Yamashita, Interplay of Pd ensemble sites induced by GaO modification in boosting CO_2 hydrogenation to formic acid, Appl. Catal. B Environ. 320 (2023), 122022.
[15] C. Wang, Y. Lei, Q. Lv, P. Wang, W. Kong, F. Wan, W. Chen, Abundant oxygen vacancies promote bond breaking of hydrogen peroxide on 3D urchin-like Pd/$W_{18}O_{49}$ surface to achieve high-performance catalysis of hydroquinone oxidation, Appl. Catal. B Environ. 315 (2022), 121547.
[16] C. Wang, Y. Li, C. Zhang, X. Chen, C. Liu, W. Weng, W. Shan, H. He, A simple strategy to improve Pd dispersion and enhance Pd/TiO_2 catalytic activity for formaldehyde oxidation: The roles of surface defects, Appl. Catal. B Environ. 282 (2021), 119540.
[17] M. Jin, H. Zhang, Z. Xie, Y. Xia, Palladium nanocrystals enclosed by {100} and {111} facets in controlled proportions and their catalytic activities for formic acid oxidation, Energy Environ. Sci. 5 (2012) 6352–6357.
[18] X. Xie, G. Gao, Z. Pan, T. Wang, X. Meng, L. Cai, Large-scale synthesis of palladium concave nanocubes with high-index facets for sustainable enhanced catalytic performance, Sci. Rep. 5 (2015) 8515–8520.
[19] M. Koohgard, M. Hosseini-Sarvari, Enhancement of Suzuki–Miyaura coupling reaction by photocatalytic palladium nanoparticles anchored to TiO_2 under visible light irradiation, Catal. Commun. 111 (2018) 10–15.
[20] S. Xie, H.C. Peng, N. Lu, J. Wang, M.J. Kim, Z. Xie, Y. Xia, Confining the nucleation and overgrowth of Rh to the {111} facets of Pd nanocrystal seeds: the roles of capping agent and surface diffusion, J. Am. Chem. Soc. 135 (2013) 16658–16667.
[21] H. Chen, B. Zhang, X. Liang, X. Zou, Light alloying element-regulated noble metal catalysts for energy-related applications, Chin. J. Catal. 43 (2022) 611–635.
[22] A. Ruditskiy, Y. Xia, The science and art of carving metal nanocrystals, ACS Nano 11 (2017) 23–27.
[23] R. Long, S. Zhou, B.J. Wiley, Y. Xiong, Oxidative etching for controlled synthesis of metal nanocrystals: atomic addition and subtraction, Chem. Soc. Rev. 43 (2014) 6288–6310.
[24] J.M. McLellan, A. Siekkinen, J. Chen, Y. Xia, Comparison of the surface-enhanced Raman scattering on sharp and truncated silver nanocubes, Chem. Phys. Lett. 427 (2006) 122–126.
[25] C.W. Liang Ma, M. Gong, L. Liao, R. Long, J. Wang, D. Wu, W. Zhong, M.J. Kim, Y. Chen, Yi Xie, and Yujie Xiong, Control Over the branched structures of platinum nanocrystals for electrocatalytic applications, ACS Nano 6 (2012) 9797–9806.
[26] B.T. Jing An, X. Zheng, J. Zhou, F. Dong, S. Xu, Y. Wang, B. Zhao, W. Xu, Sculpturing effect of chloride ions in shape transformation from triangular to discal silver nanoplates, J. Phys. Chem. C. 112 (2008) 15176–15182.
[27] S. Xu, B. Tang, X. Zheng, J. Zhou, J. An, X. Ning, W. Xu, The facet selectivity of inorganic ions on silver nanocrystals in etching reactions, Nanotechnology 20 (2009), 415601.
[28] X. Ma, F. Lin, X. Chen, C. Jin, Synergy between structure characteristics and the solution chemistry in a near/non-equilibrium oxidative etching of penta-twinned palladium nanorods, J. Phys. Chem. C. 125 (2021) 4010–4020.
[29] J. Zhang, C. Feng, Y. Deng, L. Liu, Y. Wu, B. Shen, C. Zhong, W. Hu, Shape-controlled synthesis of palladium single-crystalline nanoparticles: the effect of HCl oxidative etching and facet-dependent catalytic properties, Chem. Mater. 26 (2014) 1213–1218.
[30] Y. Chen, M. Xu, J. Wen, Y. Wan, Q. Zhao, X. Cao, Y. Ding, Z.L. Wang, H. Li, Z. Bian, Selective recovery of precious metals through photocatalysis, Nat. Sustain. 4 (2021) 618–626.
[31] J. Cao, Y. Chen, H. Shang, X. Chen, Q. Qiao, H. Li, Z. Bian, Aqueous photocatalytic recycling of gold and palladium from waste electronics and catalysts, ACS EST Eng. 2 (2022) 1445–1453.
[32] Q. Qiao, Y. Chen, Y. Wang, Y. Ren, J. Cao, F. Huang, Z. Bian, Surface modification of phosphate ion to promote photocatalytic recovery of precious metals, Chin. Chem. Lett. (2022), https://doi.org/10.1016/j.cclet.2022.03.117.
[33] L.Z.W. Niu, G. Xu, Shape controlled synthesis of single crystalline palladium nanocrystals, ACS Nano 4 (2010) 1987–1996.
[34] H. Zhao, G. Liu, Y. Liu, L. Zhou, L. Ma, Y. He, X. Zheng, J. Gao, Y. Jiang, Preparation of hollow spherical covalent organic frameworks via Oswald ripening under ambient conditions for immobilizing enzymes with improved catalytic performance, Nano Res (2022), https://doi.org/10.1007/s12274-022-4769-5.
[35] R.L. Oliveira, C.S. Oliveira, R. Landers, C.R.D. Correia, Pd nanoparticles immobilized on graphene oxide/silica nanocomposite: efficient and recyclable catalysts for cross-coupling reactions, ChemistrySelect 3 (2018) 535–543.
[36] X. Peng, Z. Cui, X. Bai, H. Lv, Bio-synthesis of palladium nanocubes and their electrocatalytic properties, IET Nanobiotechnol 12 (2018) 1031–1036.
[37] N. Li, M. Liu, B. Yang, W. Shu, Q. Shen, M. Liu, J. Zhou, Enhanced Photocatalytic Performance toward CO_2 Hydrogenation over Nanosized TiO_2-Loaded Pd under UV Irradiation, J. Phys. Chem. C. 121 (2017) 2923–2932.
[38] J.M. Walls, J.S. Sagu, K.G. Upul Wijayantha, Microwave synthesised Pd-TiO_2 for photocatalytic ammonia production, RSC Adv. 9 (2019) 6387–6394.
[39] V.J. Garole, B.C. Choudhary, S.R. Tetgure, D.J. Garole, A.U. Borse, Palladium nanocatalyst: green synthesis, characterization, and catalytic application, Int. J. Environ. Sci. Technol. 16 (2019) 7885–7892.
[40] J. Li, B. Xu, G. Liu, G. Chen, T. Zhang, F. Zhang, C. Li, Aqueous controllable synthesis of spindle-like palladium nanoparticles and their application for catalytic reduction of 4-nitrophenol, Prog. Nat. Sci. 26 (2016) 295–302.
[41] Y. Chen, L. Soler, M. Armengol-Profitós, C. Xie, D. Crespo, J. Llorca, Enhanced photoproduction of hydrogen on Pd/TiO_2 prepared by mechanochemistry, Appl. Catal. B Environ. 309 (2022), 121275.
[42] H. Zhou, B. Han, T. Liu, X. Zhong, G. Zhuang, J. Wang, Selective phenol hydrogenation to cyclohexanone over alkali–metal-promoted Pd/TiO_2 in aqueous media, Green. Chem. 19 (2017) 3585–3594.

[43] W.T. Figueiredo, R. Prakash, C.G. Vieira, D.S. Lima, V.E. Carvalho, E.A. Soares, S. Buchner, H. Raschke, O.W. Perez-Lopez, D.L. Baptista, R. Hergenröder, M. Segala, F. Bernardi, New insights on the electronic factor of the SMSI effect in Pd/TiO_2 nanoparticles, Appl. Surf. Sci. 574 (2022) 151647–151655.
[44] G. Collins, M. Schmidt, C. O'Dwyer, G. McGlacken, J.D. Holmes, Enhanced catalytic activity of high-index faceted palladium nanoparticles in Suzuki–Miyaura coupling due to efficient leaching mechanism, ACS Catal. 4 (2014) 3105–3111.
[45] C. Ao, P. Tian, L. Ouyang, G. Da, X. Xu, J. Xu, Y.-F. Han, Dispersing Pd nanoparticles on N-doped TiO_2: a highly selective catalyst for H_2O_2 synthesis, Catal. Sci. Technol. 6 (2016) 5060–5068.
[46] H.H. Shin, E. Kang, H. Park, T. Han, C.-H. Lee, D.-K. Lim, Pd-nanodot decorated MoS_2 nanosheets as a highly efficient photocatalyst for the visible-light-induced Suzuki–Miyaura coupling reaction, J. Mater. Chem. A. 5 (2017) 24965–24971.
[47] X. Zhao, J. Xie, X. Liu, X. Liu, Facilitating a high-performance photocatalyst for Suzuki reaction: Palladium nanoparticles immobilized on reduced graphene oxide-doped graphitic carbon nitride, Appl. Organo Chem. 33 (2019) 4623–4633.
[48] Y. Huang, S. Yang, M. Jiang, J. Li, L. Peng, C. Cao, W. Song, Facile synthesis of Pd nanoparticles incorporated into ultrathin crystalline g-C_3N_4 with enhanced photocatalytic performance, Cryst. Growth Des. 20 (2020) 7526–7532.
[49] Y. Zhao, Z. Huang, L. Wang, X. Chen, Y. Zhang, X. Yang, D. Pang, J. Kang, L. Guo, Highly efficient and recyclable amorphous Pd (II)/crystal Pd (0) catalyst for boosting Suzuki reaction in aqueous solution, Nano Res 15 (2021) 1193–1198.
[50] C. Wang, B. Weng, M. Keshavarz, M.Q. Yang, H. Huang, Y. Ding, F. Lai, I. Aslam, H. Jin, G. Romolini, B.L. Su, J.A. Steele, J. Hofkens, M.B.J. Roeffaers, Photothermal Suzuki coupling over a metal halide perovskite/Pd nanocube composite Catalyst, ACS Appl. Mater. Interfaces 14 (2022) 17185–17194.
[51] H. Pu, T. Zhang, K. Dong, H. Dai, L. Zhou, K. Wang, S. Bai, Y. Wang, Y. Deng, Twinned and single-crystal palladium nanocrystals for the electrooxidation of HCOOH, ACS Appl. Nano Mater. 4 (2021) 10185–10193.
[52] J.W. Hong, Y. Kim, Y. Kwon, S.W. Han, Noble-metal nanocrystals with controlled facets for electrocatalysis, Chem. Asian J. 11 (2016) 2224–2239.
[53] Z. Jiao, Z. Zhai, X. Guo, X.-Y. Guo, Visible-light-driven photocatalytic Suzuki–Miyaura coupling reaction on Mott–Schottky-type Pd/SiC, Catal., J. Phys. Chem. C. 119 (2015) 3238–3243.
[54] Y. Zhao, L. Du, H. Li, W. Xie, J. Chen, Is the Suzuki-miyaura cross-coupling reaction in the presence of Pd nanoparticles heterogeneously or homogeneously catalyzed? An interfacial surface-enhanced Raman spectroscopy study, J. Phys. Chem. Lett. 10 (2019) 1286–1291.